# Dependence of conductance on percolation backbone mass

Gerald Paul,[1,*] Sergey V. Buldyrev,[1] Nikolay V. Dokholyan,[1,†] Shlomo Havlin,[2] Peter R. King,[3,4] Youngki Lee,[1] and H. Eugene Stanley[1]

[1]*Center for Polymer Studies and Department of Physics, Boston University, Boston, Massachusetts 02215*

[2]*Minerva Center and Department of Physics, Bar-Ilan University, Ramat Gan, Israel*

[3]*BP Amoco Exploration Operating Company Ltd., Sunbury-on-Thames, Middlesex TW16 7LN, United Kingdom*

[4]*Department of Engineering, Cambridge University, Cambridge, United Kingdom*

(Received 12 October 1999)

We study $\langle \sigma(M_B,r) \rangle$, the average conductance of the backbone, defined by two points separated by Euclidean distance $r$, of mass $M_B$ on two-dimensional percolation clusters at the percolation threshold. We find that with increasing $M_B$ and for fixed $r$, $\langle \sigma(M_B,r) \rangle$ asymptotically *decreases* to a constant, in contrast with the behavior of homogeneous systems and nonrandom fractals (such as the Sierpinski gasket) in which conductance increases with increasing $M_B$. We explain this behavior by studying the distribution of shortest paths between the two points on clusters with a given $M_B$. We also study the dependence of conductance on $M_B$ above the percolation threshold and find that (i) slightly above $p_c$, the conductance first decreases and then increases with increasing $M_B$ and (ii) further above $p_c$, the conductance increases monotonically for all values of $M_B$, as is the case for homogeneous systems.

PACS number(s): 64.60.Ak, 64.60.Fr, 05.45.Df

## I. INTRODUCTION

There has been considerable study of the bond percolation cluster considered as a random-resistor network, with each occupied bond having unit resistance and nonoccupied bonds having infinite resistance [1–3]. In two dimensions, the configuration studied is typically an $L \times L$ lattice and the conductance is measured between two opposite sides which are assumed to have infinite conductance [4–16]. The backbone of the cluster is then defined as the set of bonds that are connected to the two sides having infinite conductance through paths that have no common bond.

At the percolation threshold, the backbone mass scales as $\langle M_B \rangle \sim L^{d_B}$ with $d_B = 1.6432 \pm 0.0008$ [17] and in this ''bus bar'' geometry is strongly correlated with $L$. The average conductance of the backbone as a function of $L$ has been studied extensively and has been found to scale as $\langle \sigma \rangle \sim L^{-\tilde{\mu}}$ with $\tilde{\mu} = 0.9826 \pm 0.0008$ [17].

Recently, the distribution of masses of backbones defined by two *points*, i.e., backbones defined as the set of those bonds that are connected by paths having no common bonds to two points separated by distance $r$ within an $L \times L$ lattice, has been studied [18]. This geometry has particular relevance to the oil industry where the oil field is represented by the percolation cluster and the two points represent the location of injection and production wells. One finds that when $r \ll L$, there is a very broad distribution of backbone masses for a given $r$. Figure 1 illustrates some typical percolation clusters and their backbones defined in this configuration. Because of the broad distribution of backbone masses we have the opportunity to study the conductance between these two points separated by a fixed distance $r$ as a function of the mass of the backbone defined by these points.

One might expect that, for fixed $r$, the average conductance would *increase* with increasing backbone mass because there could be more paths through which current can flow. In fact, we find that the average conductance *decreases* monotonically with increasing backbone size, in contrast with the behavior of homogeneous systems and nonrandom fractals in which conductance increases. We explain our finding by first noting that the conductance is strongly correlated with the shortest path between the two points, and then studying the distribution of shortest paths along the backbone between the two points for a given $M_B$. This analysis extends recent studies of the distribution of shortest paths where no restriction on $M_B$ is placed [19–22].

## II. SIMULATIONS

Our system is a two-dimensional square lattice of side $L = 1000$ with points $A$ and $B$ defined as $A = (L - r/2, 500), B = (L + r/2, 500)$. For each realization of bond percolation on this lattice, if there is a path of connected bonds between $A$ and $B$, we calculate (i) the length of the shortest path between $A$ and $B$, (ii) the size of the backbone defined by $A$ and $B$, and (iii) the total conductance between $A$ and $B$. We perform 100 000 realizations at the percolation threshold, $p_c = 0.5$, for each of 8 values of $r$ (1, 2, 4, 8, 16, 32, 64, and 128). We bin these results based on the value of the backbone mass, $M_B$, by combining results for all realizations with $2^n < M_B < 2^{n+1}$ and choosing the center of each bin as the value of $M_B$.

In Fig. 2(a), we plot the simulation results for the average conductance $\langle \sigma(M_B,r) \rangle$ and find that the conductance, in fact, *decreases* with increasing $M_B$. The decrease is seen more clearly in Fig. 2(b), in which we plot scaled values as discussed below.

## III. SIERPINSKI GASKET

In nonfractal systems, the conductance increases as the mass of the conductor increases. We next consider the aver-

*Electronic address: gerryp@bu.edu

†Present address: Department of Chemistry and Chemical Biology, Harvard University, Cambridge, MA 02138.

 

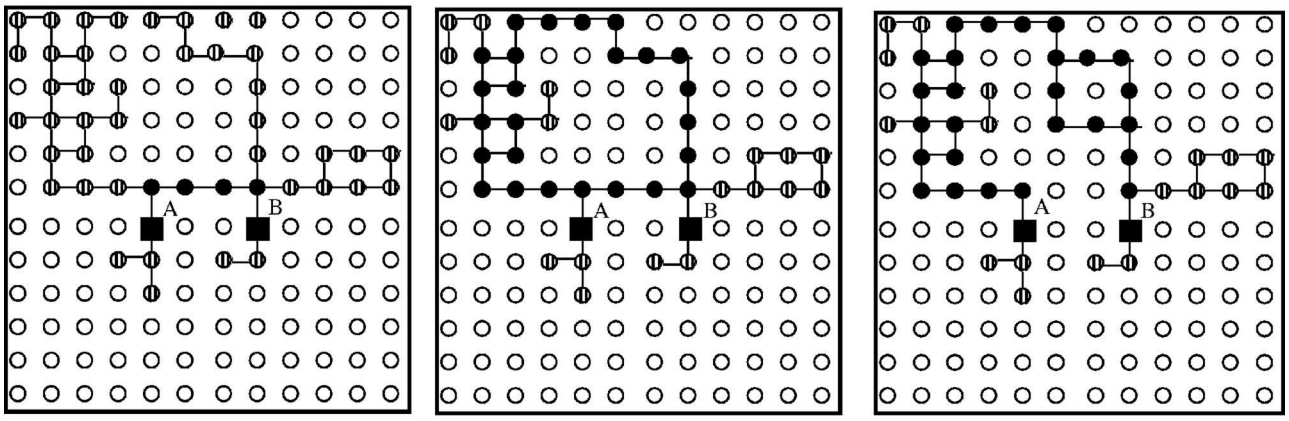


| *(a)* | *(b)* | *(c)* |
|---|---|---|
| $M_B$=6 | $M_B$=28 | $M_B$=28 |
| $l$=5 | $l$=5 | $l$=21 |
| $\sigma$=0.20 | $\sigma$=0.22 | $\sigma$=0.06 |

FIG. 1. Typical percolation clusters. The striped sites and the black sites are both part of the percolation cluster; only the black sites form the cluster backbone defined by sites *A* and *B* (black squares). Note in (a), with backbone size 6, the shortest path, $\ell$, between *A* and *B* is 5—the length of the shortest path must always be less than the backbone mass; (b) and (c) illustrate that in clusters with large backbones, the length of the shortest path between *A* and *B* can take on a broad range of values.

age conductance on the Sierpinski gasket, a nonrandom fractal, the first three generations of which are illustrated in Figs. 3(a)–3(c). Because the Sierpinksi gasket is not translationally invariant, the analog of the average conductivity between two points in the percolation cluster is the conductivity averaged over all pairs of points separated by distance $r$. At each successive generation, there are two types of pairs: (i) pairs which correspond to pairs in the previous generation (e.g., A and B) and (ii) pairs which do not correspond to pairs in the previous generation (e.g., D and E). It is obvious that as we move from one generation to the next, the conductance between pairs of type (i) increases because there are more paths between the points than in the previous generation. On the other hand, the conductance between the pairs of type (ii) are lower on average than between the pairs present in the previous generation because on average the shortest path between the two points is longer than between the pairs in the previous generation. However, for any given $r$, the shortest path between any two points has a fixed upper bound independent of the generation. Due to this bound on the shortest path, the average conductivity increases with succeeding generations. This is shown in Fig. 3(d) which shows the average conductivity calculated exactly for generations 1 to 6 for $r=1$, 2 and 4.

## IV. SHORTEST PATH DISTRIBUTION

In order to understand why the average conductance of the percolation backbone decreases with increasing $M_B$, we must (i) recognize that the conductance is strongly correlated with the shortest path [23] between the two points and (ii) study $P(\ell|M_B,r)$, the distribution of shortest paths between the two points for a given backbone mass. Hence we next create the $P(\ell|M_B,r)$ probability distribution, binning our results logarithmically by forming the average over samples centered at $\log_2\ell$.

Figure 4(a) shows the simulation results for $P(\ell|M_B,r)$ for $r=1$ for various backbone masses. The plots collapse, the only difference in the plots being the values of the upper cutoffs due to the finite backbone size. Figure 1 illustrates how the size of the backbone constrains the possible values of the shortest path. For all values of $M_B$, a section of each plot in Fig. 4(a) exhibits power law behavior. In Fig. 4(b), we show the distributions $P(\ell|M_B,r)$ for different $r$ and a given $M_B$. In Fig. 4(c) we see that when scaled with $r^{d_{\min}}$ the plots collapse, so we can write $P(\ell|M_B,r)$ in the scaling form

$$P(\ell|M_B,r)\sim\frac{1}{r^{d_{\min}}}\left(\frac{\ell}{r^{d_{\min}}}\right)^{-\psi}. \tag{1}$$

An expression for $\psi$ can be found by recognizing that we can write the well-studied distribution $P(\ell|r)$, the probability that the shortest path between two points separated by Euclidean distance $r$ is $\ell$, independent of $M_B$, as

$$P(\ell|r)=\int_{c_\ell}^{\infty}P(\ell|M_B,r)P(M_B|r)dM_B, \tag{2}$$

where (i) $P(M_B|r)$ is the distribution of backbone masses given distance $r$ between the points which determine the backbone and (ii) $c_\ell$ is the lower cutoff on $M_B$ given $\ell$. $P(M_B|r)$ has the form [18]

$$P(M_B|r)\sim\frac{1}{r^{d_B}}\left(\frac{M_B}{r^{d_B}}\right)^{-\tau_B},\quad [r\ll L], \tag{3}$$

where $d_B$ is the backbone fractal dimension and

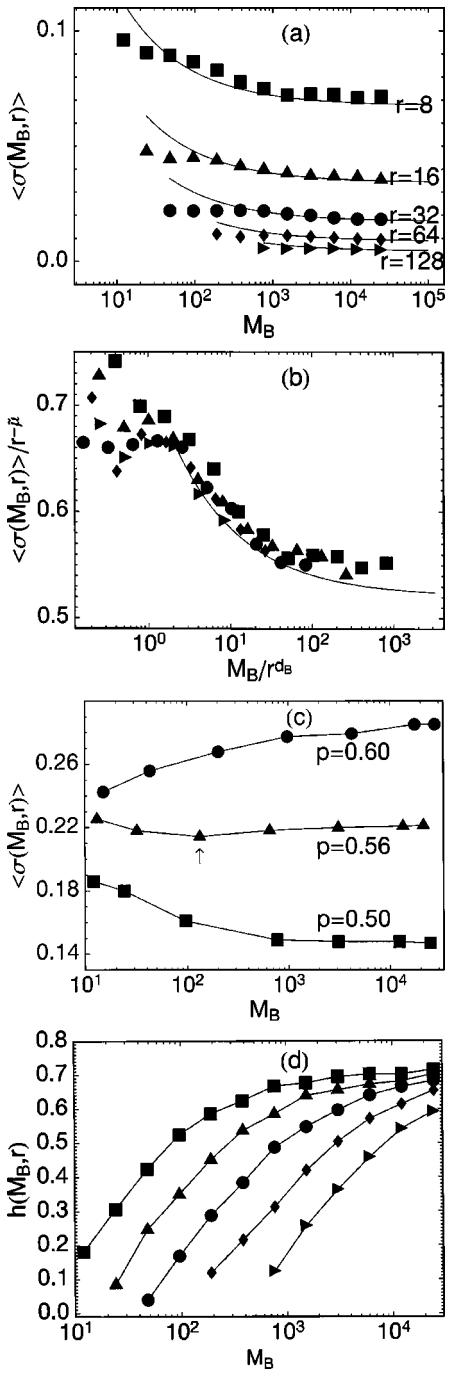


FIG. 2. Average conductance versus backbone mass. (a) Simulation results at the percolation threshold for $r=8$, 16, 32, 64, and 128, where $r$ is the distance between the two sites $A$ and $B$; the adjacent lines are the theoretical results. For large $r$, the curves for the simulation results and the corresponding curves for the theoretical results coincide for large $M_B$. (b) Plots of backbone conductance for $r=8$, 16, 32, 64, and 128, scaled in accordance with Eqs. (17) and (18). The solid line is a plot of Eq. (17) with parameters $a$ and $b$ chosen as 0.9 and 6, respectively, to best fit the values for $r=128$ (right-pointing triangles). The collapse to this line for the lower values of $r$ improves with increasing $r$. (c) Average conductance for $r=4$ for $p=0.50$, 0.56, and 0.60. For $p=0.56$, the conductance as a function of $M_B$ is not monotonic but rather has a minimum indicated by the arrow. (d) Fluctuations in conductance $h(M_B,r)=\sqrt{\langle\sigma^2(M_B,r)\rangle-\langle\sigma(M_B,r)\rangle^2}/\langle\sigma(M_B,r)\rangle$ from simulations for $r=8$, 16, 32, 64, and 128 at $p=p_c$.

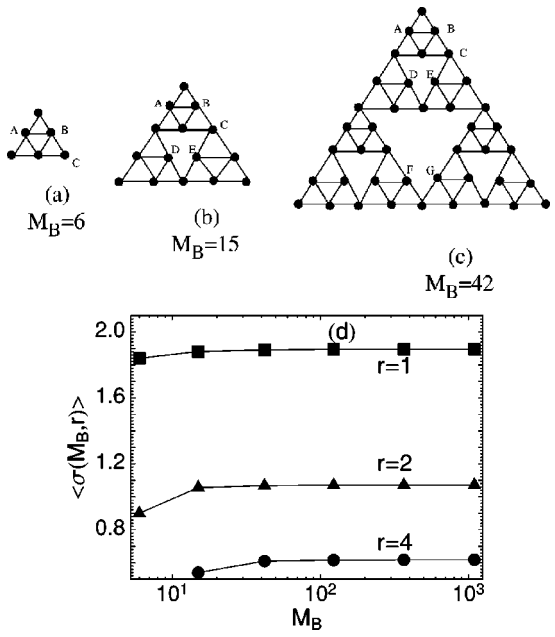


FIG. 3. (a)–(c) Three generations of the Sierpinski gasket. At each successive generation, there are two types of pairs of points: pairs which correspond to pairs in the previous generation and pairs which do not. For example, in the second generation the pairs AB and AC are present in the previous generation but the pair DE has no corresponding pair in the previous generation. Similarly, the pairs AB, AC, and DE in the third generation correspond to pairs in the second generation, but the pair FG does not. Because all points are multiply connected, the mass of the backbone between any two points in each generation is equal to the mass of the entire gasket. (d) Average conductance between all pairs of points separated by distance $r$ on the Sierpinski gasket versus the gasket mass. The points correspond to successive generations of the Sierpinski gasket.

$$\tau_B = d/d_B \tag{4}$$

is the exponent for the blob size distribution [1,24]. From Ref. [19]

$$P(\ell|r) \sim \frac{1}{r^{d_{\min}}}\left(\frac{\ell}{r^{d_{\min}}}\right)^{-g_\ell}, \tag{5}$$

where $d_{\min}$ is the fractal dimension of the shortest path. Since $\ell \sim r^{d_{\min}}$ and $M_B \sim r^{d_B}$, implying $\ell \sim M_B^{d_{\min}/d_B}$, the lower cutoff $c_\ell$ in Eq. (2) scales as

$$c_\ell \sim \ell^{d_B/d_{\min}}. \tag{6}$$

As $L \to \infty$, the upper cutoff is $\infty$ because the maximum backbone mass is not constrained by the length of the shortest path. Substituting Eqs. (3), (5), and (6) into Eq. (2), and equating powers of $r$ (or powers of $\ell$) of the left and right hand sides of the resulting equation, we find

$$\psi = g_\ell - \frac{d_B}{d_{\min}}(\tau_B - 1). \tag{7}$$

Using Eq. (4) and the values $g_\ell = 2.04$ [19,25] and $d_{\min} = 1.13$ [21,25], we find $\psi = 1.72$, in good agreement with our simulation result

$$\psi = 1.7 \pm 0.05. \tag{8}$$

## V. AVERAGE CONDUCTANCE

We can now calculate the average conductance. Since $\sigma$ is strongly correlated with $\ell$, and since $\sigma$ scales with $r$ as $r^{-\tilde{\mu}}$ and $\ell$ scales with $r$ as $r^{d_{\min}}$, we have

$$\sigma \sim \ell^{-\tilde{\mu}/d_{\min}}. \tag{9}$$

Then using the fact that $P(\ell|M_B,r) \sim \ell^{-\psi}$ we have

$$\begin{aligned} P(\sigma|M_B,r) &\sim P(\ell = \sigma^{-d_{\min}/\tilde{\mu}}|M_B,r)\frac{d\ell}{d\sigma} \\ &\sim \sigma^{(\psi-1)(d_{\min}/\tilde{\mu})-1} \\ &= \sigma^{z}, \end{aligned} \tag{10}$$

where

$$z \equiv (\psi-1)(d_{\min}/\tilde{\mu}) - 1 = -0.17. \tag{11}$$

Now $P(\ell|M_B,r)$ is nonzero only for

$$(ar)^{d_{\min}} \lesssim \ell \lesssim (bM_B)^{d_{\min}/d_B}, \tag{12}$$

where $a$ and $b$ are constants. Hence using $\langle\sigma\rangle \sim \ell^{-\tilde{\mu}/d_{\min}}$, we find $P(\sigma|M_B,r)$ is nonzero for

$$(bM_B)^{(d_{\min}/d_B)(-\tilde{\mu}/d_{\min})} = (bM_B)^{-\tilde{\mu}/d_B} \lesssim \sigma \lesssim (ar)^{-\tilde{\mu}}. \tag{13}$$

Using these bounds to normalize the distribution, we find

$$P(\sigma|M_B,r) = \frac{(z+1)\sigma^z}{(ar)^{-\tilde{\mu}(z+1)} - (bM_B)^{(-\tilde{\mu}/d_B)(z+1)}}. \tag{14}$$

Then

$$\begin{aligned} \langle\sigma(M_B,r)\rangle &= \int_{(bM)^{-\tilde{\mu}/d_B}}^{(ar)^{-\tilde{\mu}}} \sigma P(\sigma|M_B,r)\,d\sigma \\ &= \frac{z+1}{z+2}(ar)^{-\tilde{\mu}} \frac{1-\left[\dfrac{(bM_B)^{1/d_B}}{ar}\right]^{-\tilde{\mu}(z+2)}}{1-\left[\dfrac{(bM_B)^{1/d_B}}{ar}\right]^{-\tilde{\mu}(z+1)}}. \end{aligned} \tag{15}$$

Thus as $M_B$ goes to infinity, $\langle\sigma(M_B,r)\rangle$ decreases asymptotically to a constant as

$$\langle\sigma(M_B,r)\rangle \sim \frac{z+1}{z+2}(ar)^{-\tilde{\mu}}\left[1+\left[\frac{(bM_B)^{1/d_B}}{ar}\right]^{-\tilde{\mu}(z+1)}\right]. \tag{16}$$

By considering the asymptotic dependence of $\langle\sigma(M_B,r)\rangle$ on $M_B$, we can reasonably fit the simulation results by choosing the parameters $a$ and $b$ in Eq. (15) to be 0.9 and 6, respectively. Using these values for $a$ and $b$, we plot in Fig. 2(a) $\langle\sigma\rangle$ from Eq. (15) for multiple values of $r$ and find that agreement with the simulation results improves with increasing $r$. For large $r$, the curves for the simulation results and the curves for the theoretical results are coincident at large $M_B$. The poor results for small $r$ are due to corrections-to-scaling not being included in our derivation (e.g., for small $r$, there are significant corrections-to-scaling for the relations $\sigma \sim r^{-\tilde{\mu}}$ and $M_B \sim r^{d_B}$ [17]).

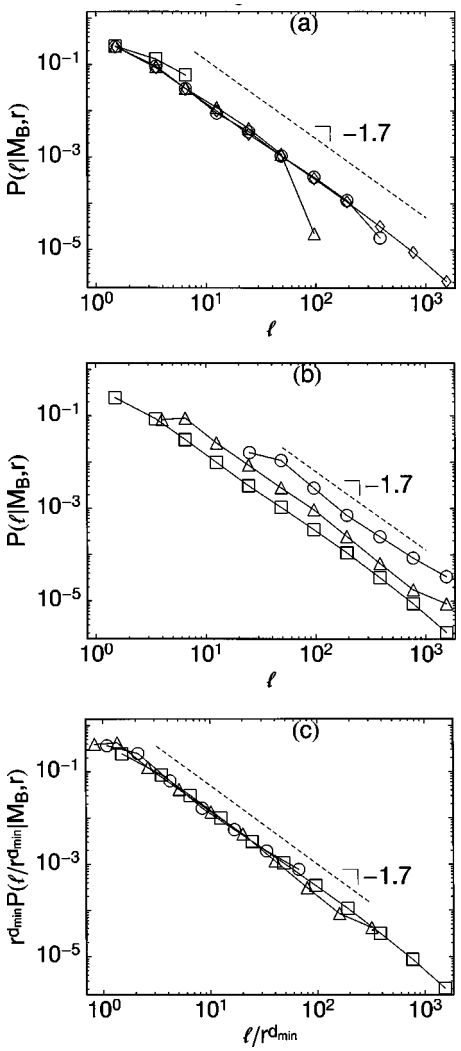


FIG. 4. Distribution of shortest paths between $A$ and $B$. (a) $P(\ell|M_B,r)$, the probability that the length of the shortest path between two points separated by distance $r$ is $\ell$ for a given backbone mass, $M_B$. All plots are for $r=1$, for values of $M_B$ of 6 (squares), 96 (diamonds), 1536 (circles), and 24 576 (triangles). The plots for the various $M_B$ differ by the points at which they cut off. (b) $P(\ell|M_B,r)$ for $r=1$ (squares), 4 (diamonds), and 16 (circles) for a single backbone size of 24 576. (c) When scaled by $r^{d_{\min}}$, the plots collapse. The dashed line is constructed to have a slope of $-1.7$; see Eq. (8).

Equation (15) can be recast in terms of the scaled variable $x \equiv M_B/r^{d_B}$ as

$$\langle\sigma(x,r)\rangle = \frac{z+1}{z+2}(ar)^{-\tilde{\mu}} f(x), \tag{17}$$

where

$$f(x)=\frac{1-\left(\frac{b}{a^{d_B}}x\right)^{-(\tilde{\mu}/d_B)(z+2)}}{1-\left(\frac{b}{a^{d_B}}x\right)^{-(\tilde{\mu}/d_B)(z+1)}}. \tag{18}$$

In Fig. 2(b), we plot the average conductance scaled in accordance with Eqs. (17) and (18). The expected collapse improves with increasing $r$ for the same reason as noted above.

Above the percolation threshold, for backbones of size larger than the correlation length, the strong correlation between the conductance and the shortest path breaks down and we expect the conductance to *increase* with the mass of the backbone, as is the case in non-random systems. This is seen in Fig. 2(c), where we plot conductance versus backbone mass for the bond occupation probabilities $p=0.56$ and $p=0.60$, which are above the percolation threshold and, for comparison, conductance *at* the percolation threshold, $p=0.50$ [26]. Figure 2(c) shows that for $p=0.60$, all backbone masses sampled are of size greater than the correlation length and the conductance increases monotonically. For $p=0.56$, the smaller backbone masses are of size less than the correlation length and Fig. 2(c) shows that the conductance initially decreases; for larger backbone masses, however, the sizes of the backbones are greater than the correlation length and Fig. 2(c) shows that the conductance then increases.

As in all problems involving strong disorder, fluctuations are significant. Using Eq. (14) we can calculate $\langle\sigma^2(M_B,r)\rangle$ at $p=p_c$. We find

$$\begin{aligned}\langle\sigma^2(M_B,r)\rangle&=\int_{(bM)^{-\tilde{\mu}/d_B}}^{(ar)^{-\tilde{\mu}}}\sigma^2P(\sigma|M_B,r)d\sigma\\&=\frac{z+1}{z+3}(ar)^{-2\tilde{\mu}}\frac{1-\left[\frac{(bM_B)^{1/d_B}}{ar}\right]^{-\tilde{\mu}(z+3)}}{1-\left[\frac{(bM_B)^{1/d_B}}{ar}\right]^{-\tilde{\mu}(z+1)}}.\end{aligned} \tag{19}$$

We next calculate the fluctuation of the average conductance,

$$h(M_B,r)=\frac{\sqrt{\langle\sigma^2(M_B,r)\rangle-\langle\sigma(M_B,r)\rangle^2}}{\langle\sigma(M_B,r)\rangle}. \tag{20}$$

In the limit $M_B\to\infty$, $h(M_B,r)$ increases to its maximum

$$h(\infty,r)=\sqrt{\frac{1}{(z+1)(z+3)}}\approx 0.65. \tag{21}$$

In Fig. 2(d), we plot $h(M_B,r)$ from our simulation data and find that, for large $M_B$, $h(M_B,r)$ approaches a value of approximately 0.7 in reasonable agreement with the value of 0.65 in Eq. (21) and confirms the fact that fluctuations are large. This is consistent with the broad distribution of shortest paths (see Fig. 4) and the strong correlation between the conductance and shortest path.

## VI. DISCUSSION

We have found through simulations that, at $p=p_c$, the average conductance of percolation backbones—defined by two points separated by Euclidean distance $r$ of mass $M_B$—decreases with increasing $M_B$. Our findings are in contrast to the behavior of homogeneous systems and nonrandom fractals. By studying the conductance of the Sierpinski gasket, a nonrandom fractal, we see that this difference is due to the fact that the shortest path between two points, separated by Euclidean distance $r$ on the Siepinski gasket, has a fixed upper bound independent of the size of the gasket, as opposed to the percolation backbone where the average length of the shortest path increases with the mass of the backbone.

A derivation, which depends only on the strong correlation between the conductance between two points and the shortest path between these points, results in a closed form expression for the conductance, Eq. (15). The agreement of Eq. (15) with the results of our simulations confirms our understanding of why the average conductance decreases with increasing backbone mass: the smaller contributions to the average conductance from the longer minimal paths possible in the clusters with larger backbone size cause the average conductance to be smaller. Our derivation was not specific to two dimensions, and should also hold in higher dimensions.

As the bond occupation probability approaches one, the behavior of the conductance must be that of a homogeneous system, for which the conductance increases monotonically for all values of $M_B$. We, in fact, confirmed this behavior and also identified a crossover regime slightly above $p_c$ in which the conductance first decreases and then increases with increasing $M_B$.

## ACKNOWLEDGMENTS

We thank M. Barthélémy and J. Andrade for helpful discussions, and BP Amoco for financial support.

[1] H.J. Herrmann, Phys. Rep. **136**, 153 (1986).
[2] T. Vicsek, *Fractal Growth Phenomena*, 2nd ed. (World Scientific Publishers, Singapore, 1992).
[3] *Fractals and Disordered Systems*, 2nd ed., edited by A. Bunde and S. Havlin (Springer, New York, 1996).
[4] S. Alexander and R. Orbach, J. Phys. (France) Lett. **43**, L625 (1982).
[5] R. Pandey, D. Stauffer, A. Margolina, and J.G. Zabolitzky, J. Stat. Phys. **34**, 427 (1984).
[6] E. Duering and H.E. Roman, J. Stat. Phys. **64**, 851 (1991).
[7] D.C. Hong, S. Havlin, H.J. Herrmann, and H.E. Stanley, Phys. Rev. B **30**, 4083 (1984).
[8] B. Derrida and J. Vannimenus, J. Phys. A **15**, L557 (1982).
[9] H.J. Herrmann, B. Derrida, and J. Vannimenus, Phys. Rev. B

**30**, 4080 (1984).
[10] J.M. Normand, H.J. Herrmann, and M. Hajjar, J. Stat. Phys. **52**, 441 (1988).
[11] R. Fogelholm, J. Phys. C **13**, L571 (1980).
[12] D.G. Gingold and C.J. Lobb, Phys. Rev. B **42**, 8220 (1990).
[13] R. Fisch and A.B. Harris, Phys. Rev. B **18**, 416 (1978).
[14] J.W. Essam and F. Bhatti, J. Phys. A **18**, 3577 (1985).
[15] A.B. Harris and T.C. Lubensky, J. Phys. A **17**, L609 (1984).
[16] A. Coniglio, M. Daoud, and H. Herrmann, J. Phys. A **22**, 4189 (1989).
[17] P. Grassberger, Physica A **262**, 251 (1999).
[18] M. Barthélémy, S.V. Buldyrev, S. Havlin, and H.E. Stanley, Phys. Rev. E **60**, R1123 (1999).
[19] N.V. Dokholyan, Y. Lee, S.V. Buldyrev, S. Havlin, P.R. King, and H.E. Stanley, J. Stat. Phys. **93**, 603 (1998); N.V. Dokholyan, S.V. Buldyrev, S. Havlin, P.R. King, Y. Lee, and H.E. Stanley, Physica A **266**, 55 (1999).
[20] M. Porto, S. Havlin, H.E. Roman, and A. Bunde, Phys. Rev. E **58**, 5205 (1998).
[21] P. Grassberger, J. Phys. A **32**, 6233 (1999).
[22] R.M. Ziff, J. Phys. A **32**, L457 (1999).
[23] R. Pike and H.E. Stanley, J. Phys. A **14**, L169 (1981).
[24] H.J. Herrmann and H.E. Stanley, Phys. Rev. Lett. **53**, 1121 (1984).
[25] H.J. Herrmann and H.E. Stanley, J. Phys. A **21**, L829 (1988).
[26] Because, above the percolation threshold, the backbone mass is strongly correlated with the system size, we create backbones of a given mass by varying the system size. The simulations of Fig. 2(c) for the plots above the percolation were obtained choosing $L = 6$, 10, 20, 40, 80, 160, and 200.